buildings

Article

A Comprehensive Approach to Earthquake-Resilient Infrastructure: Integrating Maintenance with Seismic Fragility Curves

Alon Urlainis [1] and Igal M. Shohet [2,3,*]

[1] Department of Civil Engineering, Ariel University, Ariel 40700, Israel; alonu@ariel.ac.il
[2] Department of Civil and Environmental Engineering, Ben-Gurion University of the Negev, P.O. Box 653, Beer Sheva 84105, Israel
[3] Department of Civil and Construction Engineering, Chaoyang University of Technology, Taichung 413, Taiwan
* Correspondence: igals@bgu.ac.il

Abstract: A severe seismic event can cause significant damage to infrastructure systems, resulting in severe direct and indirect consequences. A comprehensive risk-management approach is required for earthquake-resilient infrastructure. This study presents an innovative approach to seismic risk assessment and aims to integrate maintenance considerations with seismic fragility curves. The proposed methodology uniquely quantifies the impact of maintenance conditions on seismic risk, presenting a dynamic perspective of risk changes attributable to maintenance and deterioration. The methodology hinges on the hypothesis that the maintenance condition of the infrastructure and the level of deterioration impacts the seismic resilience of the infrastructure. The methodology synergizes the Building Performance Index (BPI) and the deterioration over time to evaluate their cumulative effect on fragility curves to estimate the infrastructure's total risk over the lifecycle (TRLC). This proposed methodology is demonstrated through a case study of a low-voltage substation in Bik'at HaYarden, Israel. A Monte Carlo simulation was carried out for the specific conditions of the analyzed substation. A comprehensive sensitivity analysis was performed to understand better the effect of maintenance conditions over time on the TRLC. Key insights reveal a statistically significant correlation between infrastructure performance and maintenance and their consequential impact on the TRLC. Notably, declining maintenance conditions intensify seismic risk uncertainties. The research proposes to researchers, stakeholders, and decision-makers a novel comprehensive perspective on the indispensability of maintenance for seismic risk management and mitigation.

Keywords: building performance indicator; fragility curves; maintenance; risk; seismic resilience

Citation: Urlainis, A.; Shohet, I.M. A Comprehensive Approach to Earthquake-Resilient Infrastructure: Integrating Maintenance with Seismic Fragility Curves. *Buildings* **2023**, *13*, 2265. https://doi.org/10.3390/buildings13092265

Academic Editors: De-Cheng Feng, Ji-Gang Xu and Xuyang Cao

Received: 16 August 2023
Revised: 31 August 2023
Accepted: 4 September 2023
Published: 6 September 2023

1. Introduction

Infrastructure systems, such as transportation, energy, water, wastewater, telecommunications, healthcare facilities, financial systems, educational institutions, and emergency services, are essential for the continuous performance of modern society and the economy in ordinary times and during emergencies. Infrastructures are complex systems composed of structural and nonstructural components [1]. Damage to a single component can lead to the disruption of the entire system, and the latter implies that the vulnerability of the infrastructure depends on its layout and functional–topological relationships. Therefore, when considering the seismic performance of the system, it is crucial to consider the vulnerability at the component level.

A severe seismic event can cause significant damage to infrastructure systems, resulting in severe direct and indirect consequences, as was recently catastrophically demonstrated in the Turkey–Syria earthquake [2,3]. These outcomes can trigger cascading and rippling effects across various sectors, leading to economic losses, physical destruction, and human casualties [1]. Therefore, the resilience of infrastructures after seismic events is a critical aspect of ensuring the safety and functionality of communities.

Infrastructure resilience is an increasingly important multidisciplinary field that integrates technical, social, and economic dimensions to prepare for, respond to, and recover from disasters. Cimellaro et al. presented an analytical framework [4] in which resilience is understood as a time-dependent recovery process influenced by societal preparedness and public policies. Rasulo et al. extended this to the seismic resilience of road networks, emphasizing the critical role of bridges in maintaining network functionality [5]. Bocchini et al. [6] argued that resilience and sustainability are complementary, both involving lifecycle analyses and social–economic impacts. Those works suggest that resilience is not just about recovery but also about adaptive evolution in the face of disruptions, making it a key consideration for both policy and engineering decisions.

Seismic fragility curves are a common method for assessing the expected damage of various types of infrastructure due to seismic events. The fragility curve represents the probability that a component or system will reach or exceed a given damage state as a function of an earthquake's intensity-measure (IM) parameter, such as peak ground acceleration (PGA), peak ground velocity (PGV), and peak ground displacement (PGD) [7]. Fragility curves can be used for individual components or the entire systems [8,9].

The general formulation of a fragility function of a structure or system is framed as a lognormal cumulative distribution function (CDF) [10–12]. To accurately define this function, it is essential to determine two parameters: the median capacity of the component to resist the damage state (θ_{ds}) and the standard deviation of the capacity (β_{ds}), as presented in Equation (1).

$$P[DS \geq ds|IM = x] \ = \Phi\left(\frac{\ln(x/\theta_{ds})}{\beta_{ds}}\right); ds \in \{1, 2, \ldots N_{DS}\} \tag{1}$$

where P stands for a conditional probability of being at or exceeding a particular damage state (DS) for a given seismic intensity and x is defined by the earthquake-intensity measure (IM).
where,

DS: The uncertain damage state of a particular component, {0, 1, . . .N_{DS}};
ds: A particular value of the DS;
N_{DS}: The number of possible damage states;
IM: Uncertain excitation, the ground-motion-intensity measure (i.e., PGA, PGD, or PGV);
X: A particular value of the IM;
Φ: The standard cumulative normal distribution function;
θ_{ds}: The median capacity of the component to resist a damage state ds measured in terms of the IM;
β_{ds}: The logarithmic standard deviation of the uncertain capacity of the component to resist a damage state ds.

In instances where more than one damage state is defined, the damage states are ordered by damage severity (from the least severe to the most severe damage), and the fragility function defines the cumulative probability of being in a specified damage state. Equation (2) expresses the distribution of probabilities of exceeding different levels of damage for a given IM value.

$$P(DS = ds_i|IM) = \begin{cases} 1 - P(DS \geq ds_i|IM) & i = 0 \\ P(DS \geq ds_i|IM) - P(DS \geq ds_{i+1}|IM) & 1 \leq i \leq n-1 \\ P(DS \geq ds_i|IM) & i = n \end{cases} \tag{2}$$

Many studies have focused on the development and application of seismic fragility curves for different types of infrastructure, including different types of buildings [13–15] and special structures, such as churches [16], bridges [17], different steel tanks [18–20], power grids [21], water networks [22], transportation infrastructure [23], oil-pumping stations [9], and concrete dams [24]. The fragility curves are developed regarding various factors, such as the geometry of the elements, the materials, the overall capacity of the system, and several other factors. However, one aspect that has received less attention in developing seismic fragility curves is the integration of maintenance considerations with seismic resistance.

Maintenance of infrastructures is critical to ensuring durability, functionality, and effectiveness [25]. Maintenance activities include routine inspections, required repairs and replacements, and upgrades to maintain the structural integrity, reliability, and performance of the infrastructure system. Several studies have explored different aspects of infrastructure maintenance, including planning and scheduling [26,27], maintenance expenditures [28,29], maintenance practice challenges [30], monitoring, and climate-related disaster planning in asset management [31].

The maintenance level of the infrastructure is a significant factor that can impact the vulnerability of the infrastructure system to seismic events [32,33]. Furthermore, the functionality of the infrastructure depends on the continuous performance of each component within the system. Therefore, the system components' maintenance level can significantly impact the seismic vulnerability of the entire system. Proper maintenance can prevent deficiencies or wear and tear, ensure the system is in a suitable condition, and better resist seismic impact. In contrast, improper maintenance can increase the probability of failure and compromise the system's seismic resistance. In addition, most maintenance practices often do not consider the vulnerability of the components to seismic events, resulting in a gap between maintenance operations and seismic-risk-reduction strategies. Thus, maintenance activities affect seismic performance and may foster resilience to seismic events.

Shohet [34] introduced a Building Performance Indicator (BPI) in order to quantify the performance of an entire building, relying on the performance assessment of its particular systems and components. The methodology introduces the implementation of systematic rating scales to evaluate the condition of the building's components and combining them using lifecycle cost principles. Subsequently, the overall state of the infrastructure is assessed via the BPI, which is derived from the weighted average of the scores attributed to the various building systems and components and their LCC significance in the overall building LCC. The BPI considers several criteria, such as the actual physical performance of the systems, the frequency of failures in building systems, and the actual preventive maintenance carried out on the building structure and systems.

Several studies aimed to consider maintenance parameters regarding seismic vulnerability. Manos et al. [35] discussed maintenance issues related to the structural integrity of stone-masonry bridges. However, no analytical process was introduced. Crespi et al. [36] investigated the seismic performance of reinforced-concrete bridges under several corrosion scenarios, as the corrosion levels represent the maintenance status. Zanini et al. [37] analyzed the seismic vulnerability of corroded bridges in transport networks by developing fragility curves that accounted for steel-reinforcement corrosion. Soltani et al. [38] presented the relationship between the maintenance cost and the engineering-demand parameters (EDPs) for the case of infill walls. Tecchio et al. [39] intended to provide seismic fragility models for two generalized classes of single-span masonry arch bridges considering the material degradation and longitudinal cracks [39]. It was found that the seismic fragility of masonry bridges increases when the effects of degradation are considered, as the loss of material was found to be the most influential defect. Moreover, an integrated approach that includes infrastructure maintenance was presented by [40]. The paper proposed an integrated maintenance–safety framework, demonstrating a strong correlation between maintenance and safety levels. A case study of a public facility validated the framework, emphasizing unified maintenance–safety procedures to enhance facility performance.

Various analytical frameworks and indicators have been proposed to enable risk-informed decision-making for the seismic mitigation of critical infrastructure. Wang et al. presented a methodology integrating adjusted fragility curves into risk functions to evaluate mitigation strategies quantitatively [41]. Furthermore, Urlainis and Shohet incorporated fragility analysis with fault-tree modeling to assess risk expectancy and proposed a Risk Mitigation to Investment Ratio indicator for prioritizing retrofitting alternatives based on risk-reduction cost-effectiveness [42]. Wei et al. developed a benefit–cost analysis approach to evaluate the economic feasibility of seismic retrofitting in moderate-seismicity regions, demonstrating its application through a case study in Tiberias, Israel [43]. These studies exemplify different tools and techniques to appraise seismic risk and guide mitigation decisions through analytical indicators.

Moreover, it should be noted that the risk assessment for infrastructures with more than one component is a complex task. Nuti et al. developed a model to evaluate the seismic fragility of electric power network components and the overall network capability considering component damage states, power flow, and soil conditions. The analysis emphasized the importance of accurate geotechnical modeling for predicting seismic response and safety [44]. Furthermore, Nuti et al. (2010) discussed modeling approaches for the seismic risk assessment of large-scale-infrastructure networks, including electric power, water, and transportation systems. The analysis emphasized need for network-level modeling to capture component interactions and cascading failures. Case studies demonstrated Monte Carlo simulations for the probabilistic seismic analysis of networks [45].

Rasulo et al. presented a modeling framework combining GIS, seismic risk analysis, and traffic simulation to assess direct and indirect earthquake impacts on road networks. The methodology was demonstrated through a case study of a bridge network in Central Italy, emphasizing the importance of calibrated traffic models for quantifying postseismic network accessibility and delays [46].

This review sheds light on the gap between the analytical models in seismic resistance and the analytical–empirical models in maintenance that can be integrated into a comprehensive synergetic framework. Therefore, this research aims to establish fragility curves that integrate seismic and maintenance factors, thereby enabling a comprehensive performance methodology.

This study proposes a comprehensive approach toward earthquake-resilient infrastructures by incorporating maintenance factors into the seismic-risk-analysis process. By incorporating the maintenance-level data into the seismic fragility curves, this paper hypothesizes that an advanced, innovative, and reliable representation of the system vulnerability will be produced. By integrating maintenance considerations with seismic fragility curves, infrastructure owners and managers can make informed decisions regarding maintenance strategies and investments to enhance the resilience of their assets.

The uniqueness of our work lies in the pioneering integration of maintenance considerations with seismic fragility curves, a feature which is distinctly absent in the existing literature. This groundbreaking consolidation allows us to present a more comprehensive, holistic view of infrastructure resilience that goes beyond immediate seismic resistance to include long-term sustainability through effective maintenance. In traditional seismic fragility models, the focus is primarily on understanding how infrastructure responds to earthquakes without considering how ongoing maintenance activities can impact this response. Our integrated approach aims to bridge this gap.

2. Integration of the Building Performance Indicator with Seismic Fragility Curves

2.1. Baseline Seismic Fragility Curves

The baseline fragility curves were developed based on typical methodologies without considering the maintenance. Those curves can be developed for a specific component, a generic system, or an exclusive infrastructure system layout. Fragility-curve parameters for a specific component can be found in the FEMA P-58 component fragility function database (FEMA database [47]). A generic system or infrastructure type provides different types of buildings and infrastructure-fragility parameters. For an exclusive layout of infrastructure, Urlainis and Shohet developed a comprehensive methodology based on fault-tree analysis [9]. In each of these cases, the baseline fragility curves provide a probabilistic measure of the structure's seismic vulnerability without considering the influence of maintenance. These curves serve as a benchmark against which maintenance effects can be evaluated in the subsequent steps of the integration process. The baseline seismic fragility curves are formulated in Equations (1) and (2).

2.2. *Building Performance Indicator of Critical Infrastructures*

In this step, the determination of the maintenance state of the infrastructure is performed. This includes evaluation of the physical condition, the quality of materials, age, the level of wear and tear, and the maintenance activities performed. This determines the infrastructure's maintenance state, which can be crucial for evaluating its seismic vulnerability.

It aims to consider the two main parameters: (1) the current maintenance condition of the infrastructure and the (2) level of deterioration over the years. For that purpose, two coefficients are attributed for the infrastructure: M_c for the maintenance level and D_c for deterioration.

To validate the proposed model, its representation of maintenance and deterioration impacts on seismic responses was cross-referenced with findings by [36] concerning the effects of the corrosion of steel on the seismic capacity of bridges. Crespi [36] delineated various risk indices' values acquired across different deterioration scenarios over a lifecycle and elucidated their implications on the seismic capacity. Consequently, in this study, the model's coefficients were calibrated and validated using that dataset.

2.2.1. The Maintenance Coefficient

The maintenance-level coefficient M_c is a quantitative measure that expresses the informed state of the maintenance of a component, a system, or the entire infrastructure. It provides a standardized metric to measure the extent to which maintenance activities have been performed on a particular infrastructure.

The maintenance coefficient (M_c) can be evaluated according to maintenance records, condition assessments, or expert evaluations. In general, it aims to represent various factors, such as:

- Frequency of Maintenance: how regular maintenance activities are performed. Regular, scheduled maintenance usually indicates a higher maintenance level.
- Quality of Maintenance: the thoroughness and effectiveness of maintenance procedures. High-quality maintenance that addresses potential issues proactively contributes to a higher maintenance level.
- Maintenance History: past maintenance records, including any instances of delayed or skipped maintenance, which might impact the current condition of the component or system.
- Current Condition: the current physical condition of the component or system, assessed through inspections or condition-monitoring systems. This could include factors such as wear and tear, damage state, degradation, etc.
- Performance Metrics: operational data indicating the performance of the component or system. This might include efficiency, reliability, or failure rates, among other metrics.

In this research, the maintenance-condition coefficient is calculated based on the evaluation of the system using the Building Performance Indicator (BPI). The BPI is calculated as a compounded score of several components of the infrastructure system.

$$\mathrm{BPI} = \sum_{\mathrm{n}=1}^{\mathrm{N}} \mathrm{P_n} \cdot \mathrm{W_n} \tag{3}$$

where,

BPI—Building Performance Indicator (0–100);
$\mathrm{P_n}$—Performance level for system n (on a scale of 0 to 100);
$\mathrm{W_n}$—Weight of system n in the BPI.

The BPI value reflects the performance level of the building, where a lower value indicates poor or neglected maintenance and a higher value represents the well-maintained condition. The BPI is designed to account for various aspects of maintenance, including the frequency and quality of maintenance activities, current condition, and additional metrics, such as the repair rate and failure rate. Shohet [34] divided the BPI values into the following general categories:

- BPI > 80 indicates that the state of the building and its resultant performance are good or better;
- 70 < BPI < 80 indicates that the state of the building is such that some of the systems are in marginal condition, i.e., some preventive maintenance measures must be taken;
- 60 < BPI < 70 indicates deterioration of the building, i.e., preventive and breakdown maintenance activities must be carried out;
- BPI < 60 means that the building is run-down.

In this study, the BPI values act as an indicator of the system's maintenance level. The maintenance coefficient, represented as M_c, is elaborated upon in Equation. This equation delineates a direct linear relationship between the maintenance coefficient and the building's performance. As the BPI rises, signifying enhanced building performance, the maintenance coefficient correspondingly increases, denoting improved maintenance conditions. This relationship is based and validated on the findings presented in [36].

$$\mathrm{M_c} = 0.01 \cdot \mathrm{BPI} + 0.1 \tag{4}$$

2.2.2. The Rate of the Deterioration-over-Time Coefficient

Despite even rigorous maintenance practices, all infrastructural elements experience a certain level of degradation due to various factors, such as weather, an intensive service regime, the design lifecycle, and inherent material properties. The deterioration-over-time coefficient $D_C(t)$ is a measure that captures the progressive degradation or wear-and-tear of a component or system in an infrastructure due to factors such as age, service regime, environmental conditions, and inherent material properties. It essentially encapsulates the natural aging process and lifecycle deterioration of infrastructure elements, even under ideal maintenance practices. The indicator is time-dependent, as the indicator value changes as a function of the duration since the infrastructure was built or renovated. Several factors impact on the deterioration-over-time indicator $D_C(t)$, such as:

- Age of the System: the period since the component or system was installed or last renovated. Older components typically show more signs of wear and tear.
- Designed Lifecycle: the lifecycle for which the component or system was initially designed also impacts its rate of deterioration. Components designed for a longer lifespan may have higher durability and slower deterioration compared to those designed for shorter lifecycles.
- Service regime: the degree and nature of usage can accelerate the deterioration process.
- Environmental Conditions: exposure to harsh environmental conditions, such as temperature fluctuations, humidity, salinity, etc., can influence the rate of deterioration.
- Material Properties: different construction materials have different inherent lifespans and susceptibility to deterioration. For instance, steel might corrode over time while concrete may experience spalling, cracking, and corrosion.

The proposed model for assessing infrastructure deterioration over time is implemented in two distinct steps: initially, the deterioration score of the infrastructure is established, considering various construction properties, such as material durability, environmental conditions, and the service regime. Subsequently, the deterioration coefficient, which encapsulates the rate of infrastructure degradation, is determined using an exponential decay model, thereby establishing a time-dependent function that accurately represents the infrastructure's deterioration over time.

The infrastructure deterioration score is evaluated on the base of three factors: the service regime (SR), environmental conditions (EC), and the infrastructure material properties

(MP). Each factor is scored on a scale from 1 to 5, with 1 representing the most favorable conditions and 5 representing the most unfavorable conditions (e.g., heavy usage, harsh environmental conditions, materials highly susceptible to deterioration). The detailed elaboration of the scoring metric is provided in the Appendix A.

The model assigns a weight to each factor, denoted as W_{SR}, W_{EC}, and W_{MP}, reflecting its relative contribution to the rate of the building's systems deterioration. These weights can be adjusted based on specific circumstances and expert judgment, and can be inferentially statistically analyzed. In this formula, Equation (5), S is the weighted sum of the factor scores and P is the performance score, Equation (6), normalized to a range from a_0 to 99. As a_0 is a calibration coefficient, it stands for the performance score for perfect conditions.

$$S = SR \cdot W_{SR} + EC \cdot W_{EC} + MP \cdot W_{MP} \tag{5}$$

$$P = \mathrm{a}_0 + (99 - \mathrm{a}_0) \cdot \left[\frac{S - (W_{SR} + W_{EC} + W_{MP})}{4 \cdot (W_{SR} + W_{EC} + W_{MP})} \right] \tag{6}$$

where,

SR: Service-regime-intensity factor;
EC: Environmental-conditions factor;
MP: Material-properties factor;
W_{SR}, W_{EC}, W_{MP}: Weights associated with each factor;
a_0: Calibration coefficient for the performance score for perfect conditions;
P: Performance score of the infrastructure.

The proposed coefficient for infrastructure deterioration over time is formulated in Equation (7). This equation represents an exponential decay model, where $D_c(t)$ is the deterioration-over-time coefficient at a given time t. This coefficient provides a quantifiable measure of the infrastructure's state at a specific time, with a higher value indicating a higher level of deterioration. The variable t represents the number of years elapsed since the start of the evaluation period. P_0 is the initial performance, typically set at 1.0, representing the infrastructure's state at the start of the evaluation period. The performance score is represented by P, ranging between a_0 and 99. LC represents the designed lifecycle of the infrastructure. The equation calculates the deterioration-over-time coefficient as an exponential function of time, with the rate of increase determined by the performance score and the designed lifecycle. This model provides a simple yet effective way to assess the infrastructure deterioration over time.

$$D_c(t) = P_0 \cdot e^{-P \cdot \frac{t}{LC} \cdot 100} \tag{7}$$

where,

$D_c(t)$: Deterioration-over-time coefficient at time t;
t: Time. The number of years since the start of the evaluation period;
P_0: Initial performance (usually set a 1.0);
LC: Designed lifecycle of the infrastructure.

2.2.3. Integrating Uncertainty to the Model

In the field of infrastructure management, it is crucial to acknowledge that maintenance conditions are not deterministic. They are subject to inherent uncertainties and temporal variations. To include these uncertainties within the proposed model, the coefficient M_c, which signifies the maintenance condition, can be defined as a lognormally distributed random variable. The lognormal distribution is characterized by two parameters: the mean (μ_{M_c}) and the standard deviation (σ_{M_c}). The mean, μ_{M_c}, a function of the Building Performance Indicator (BPI), expresses the relationship between the m coefficient and the building's performance. The standard deviation, σ_{M_c}, represents the uncertainty in the maintenance condition. It can be estimated from historical data, surveys, expert opinion, or as a combination in a hybrid approach. In situations where such resources are unavailable, a heuristic approach can be adopted, setting the standard deviation as a fraction of the mean (10–20%).

The uncertainty associated with the deterioration over time should also be considered. The deterioration-over-time coefficient, $D_c(t)$, which quantifies the rate of infrastructure degradation, can be modeled as a lognormally distributed random variable. This distribution can be determined based on historical data, expert opinion, or a hybrid approach, providing a probabilistic measure of the infrastructure's state at a specific time. The lognormal distribution is defined by two parameters: the mean μ_{D_c} and the standard deviation σ_{D_c}, which represent the expected value and the uncertainty of the deterioration coefficient, respectively. This approach enhances the robustness of the model, making it more adaptable to real-world scenarios and better equipped to capture the complex dynamics of infrastructure deterioration over time.

The lognormal distribution is proposed for this model due to its inherent properties. It is characterized by two parameters: the mean μ and the standard deviation σ. These parameters enable the distribution to encapsulate the inherent uncertainty and variability in the deterioration process and maintenance conditions. Additionally, the lognormal distribution is defined exclusively for positive real numbers. This aligns with the context of the deterioration coefficient and the performance score, which cannot assume negative values. This positivity property ensures that the modeled quantities adhere to their logical and physical constraints.

2.2.4. Calibration and Validation of the Coefficients

A crucial aspect of the proposed methodology is the calibration and validation of the maintenance coefficient (M_c) and deterioration coefficient (D_c). At present, there are limited datasets directly relating the observed seismic damage to the quantified maintenance conditions of infrastructure components or systems. Further research should prioritize the compilation of empirical seismic–maintenance datasets across diverse infrastructure typologies, components, and seismic events. These empirical datasets can enable continuous calibration and validation of the coefficients underlying the fragility models.

Moreover, it is essential to leverage ongoing advancements in complementary fields to refine the calibration methodology. For instance, integrating machine-learning techniques such as artificial neural networks (ANNs) could assist in analyzing large empirical datasets and identifying key correlations, and coupling ML predictions with numerical analysis provides a means for the virtual validation of deterioration models [48,49]. Transfer-learning methods may also help overcome limitations posed by small sample sizes [50]. Dabiri et al. [51] developed ML-based models using decision trees, ANNs, and other techniques to predict the dispersion and median PGA parameters of building fragility curves. Training on a database of 214 published datasets demonstrated the accurate prediction of fragility parameters based on key building inputs, such as material, geometry, period, etc.

By unifying empirical data collection with cutting-edge analytical techniques, the accuracy and robustness of the coefficients can be enhanced incrementally. The fragility models can be updated and validated in turn. This can enable the methodology to become more precise and comprehensive over time through continual empirical grounding and analytical refinement.

2.3. Adjust Fragility Curves Based on the Maintenance Level and the Rate of Deterioration

In this step, the baseline seismic fragility curves are adjusted based on the maintenance level and the rate of deterioration of the infrastructure or the components. For instance, well-maintained structures may be less vulnerable to earthquakes, resulting in shifts in their fragility curves. In contrast, structures with poor or neglected maintenance may show increased vulnerability, leading to adjustments in their fragility curves. The adjustment process is intended to account for two specific parameters: the current state of the component or a system, based on the maintenance-level indicator (M_c), and the rate of the deterioration-over-time indicator ($D(t)$).

In this step, the baseline fragility curve parameters for each damage state *i* are updated. A general adjustment of θ_{ds} and β_{ds} is implemented in expression (8):

$$\theta'_{ds_i}(t) = \theta_{ds_i} \cdot f_{\theta_i}(M_c, D_c(t)) = \theta_{ds_i} \cdot D_c(t) \cdot M_c \tag{8}$$

2.4. Dynamic Update of the Fragility Curves

The previous steps change the infrastructure state over time due to maintenance-level and time-dependent deterioration, and it is essential that the seismic fragility curves will be reupdated to reflect these changes. Thus, this step implements the re-evaluation and reassessments of the infrastructure's vulnerability and subsequent adjustments to the fragility curves. Furthermore, the maintenance parameters (the maintenance-level indicator (M_c) and the deterioration-over-time indicator (D_c)) must be monitored and updated correspondingly. The process will be iterative, as new data will be available and enable the refinement of the maintenance indicators and the fragility parameters.

2.5. Assessment of the Seismic Risk

In this step, the seismic risk expectancy of the infrastructure, taking into account the maintenance indicators, is calculated. Equation (9) expresses the cumulative risk expectancy for a T-years lifespan of the system, denoted as the $TRLC$. This expression comprehensively captures the overall risk the system may encounter due to earthquake events throughout its design lifecycle. The $TRLC$ is calculated based on possible seismic scenarios, their occurrence probability, and the expected consequences. Furthermore, R_U expresses the overall consequences that are expected in case of complete damage to the system, quantified in terms of cost (US$). Figure 1 presents a general flow of the methodology.

$$\text{TRCL} = \left[\sum_{t=1}^{T} \sum_{m=1}^{IM} \left(\sum_{i=1}^{N} P(ds_i|IM) \cdot DR_{ds_i}\right) \cdot PE_A(IM)\right] \cdot R_U \tag{9}$$

$$R_U = \left(\sum C_R + \sum C_D\right) \cdot C_I \tag{10}$$

where,

$TRLC$—Total risk for the infrastructure design life cycle;
DR_{ds_i}—Damage rate of damage state i;
$P(ds_i|IM)$—Conditional probability of being in a certain damage state i for a given IM;
T—Design lifecycle;
$PE_A(IM)$—Annual rate of exceedance of a given IM;
C_R—Repair cost (US$);
C_D—Direct loss (US$);
C_I—Indirect loss coefficient;
R_U—Overall consequences (US$).

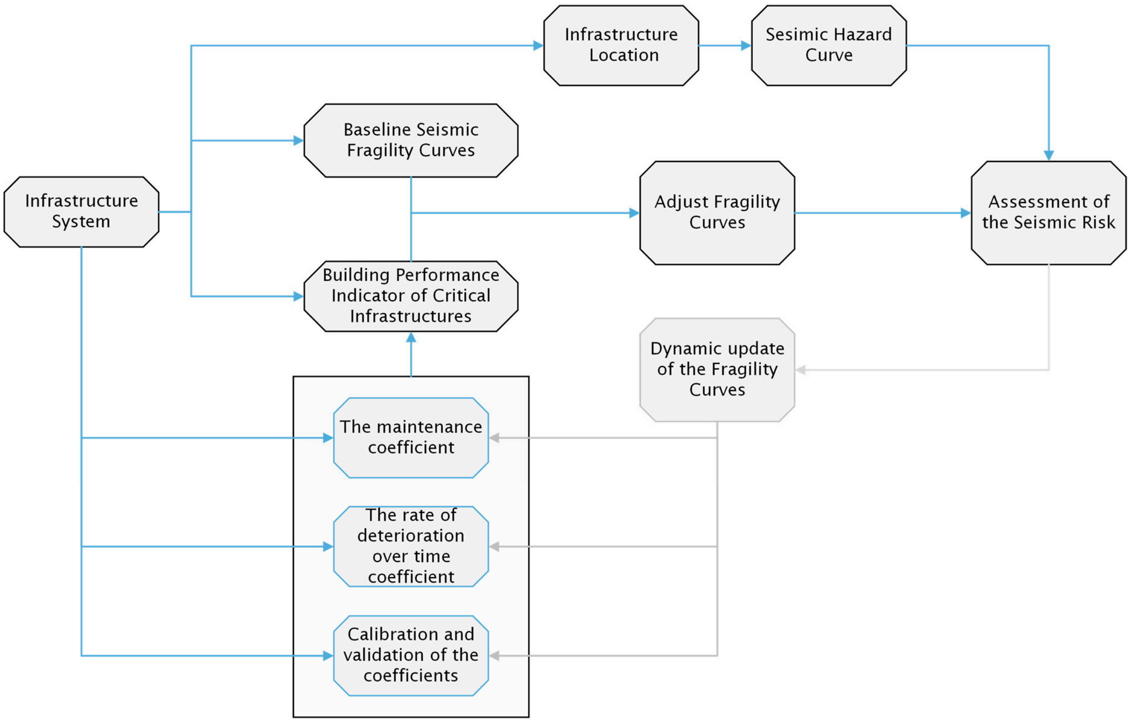

Figure 1. Methodology flowchart (the gray arrows represent the dynamic update of fragility curves based on routine inspection).

3. Case Study

In this section, the methodology is demonstrated through a case study of an energy building. Due to security concerns, the detailed plan and the actual location of the building cannot be disclosed. However, for the purpose of demonstrating the methodology, an alternative location will be used throughout this case study.

The infrastructure under investigation in this study is a low-voltage substation for a hi-tech industrial complex. A low-voltage substation is primarily designed to distribute electrical power at a lower voltage level from the main power grid to end-use consumers. It acts as an intermediary, ensuring the efficient transmission of power to various units or buildings within a complex. In the context of our case study, the substation is housed within a one-story, shear-moment reinforced-concrete structure. This facility is equipped with essential components, such as transformers, switchgear, circuits, and an uninterruptible power supply (UPS). Additionally, it includes a comprehensive HVAC system and a comprehensive fire-detection and suppression system to ensure safety and functionality. The substation is in the region of Bik'at HaYarden in Israel.

3.1. Baseline Seismic Fragility Curves

The baseline seismic fragility curve for the substation is defined based on the HAZUS methodology. The fragility curve includes four damage states: slight, moderate, extensive, and complete. Each of these damage states is associated with a set of parameters and conditions that are defined according to the HAZUS methodology [52]. The parameters of each state, including the median (θ_i) and standard deviation (β_i), of the lognormal cumulative distribution function are included (Figure 2). Furthermore, each damage state is coupled with a specific damage ratio. In our case, the total replacement value of the substation is evaluated to be 10 million US dollars. Detailed information about the damage states, descriptions, the associated parameters, and the corresponding damage ratios, are elaborated in Tables 1 and 2.

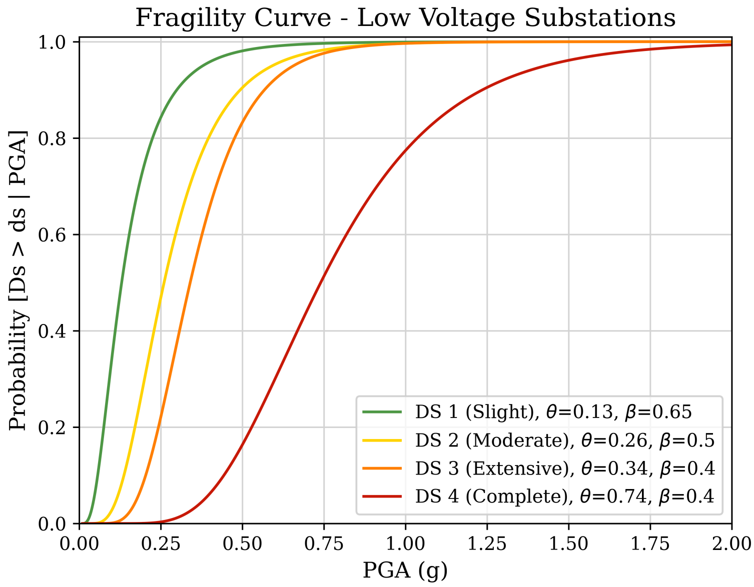

Figure 2. Fragility curve of a low-voltage substation.

Table 1. Baseline fragility curve parameters and damage ratio.

Damage State		θ_i	β_i	**Damage Ratio**
DS1	Slight	0.13	0.65	0.05
DS2	Moderate	0.26	0.50	0.11
DS3	Extensive	0.34	0.40	0.55
DS4	Complete	0.74	0.40	1

Table 2. Damage state description.

Damage State		**Description**
DS1	Slight	Failure of 5% of the disconnect switches or circuit breakers, or by the building being in the slight damage state
DS2	Moderate	Failure of 40% of disconnect switches, circuit breakers, or current transformers, or by the building being in the moderate damage state
DS3	Extensive	Failure of 70% of disconnect switches, circuit breakers, current transformers, or transformers, or by the building being in the extensive damage state
DS4	Complete	Failure of all disconnect switches, all circuit breakers, all transformers, or all current transformers, or by the building being in the complete damage state

3.2. Analysis of Building Performance Coefficients

The building maintenance conditions were surveyed several times, and the total score of the Building Performance Indicator (BPI) from six recorded surveys is detailed in Table 3. The surveys included records on building structure, exterior envelope, interior finishes, power supply, water and sewerage systems, HVAC (heating, ventilation, and air conditioning), fire detection and suppression, elevators and escalators, and peripheral infrastructure.

The average BPI score is 85.50, with a standard deviation of 1.58. In this case study, it is intended to consider the uncertainty of the maintenance conditions. Therefore, the BPI score is determined as a lognormal distributed variable, as described in Equation (11). Based on the dataset with an observed mean of 85.5 and a standard deviation of 1.58, the parameters of the normal distribution were determined. The mean of the normal distribution, corresponding to the logarithm of the variable, is found to be approximately

4.448, and the standard deviation of the normal distribution is identified as approximately 0.018 (as described in Equation (11)).

$$BPI \sim logN\ (\ \mu_{BPI} = 4.448, \sigma_{BPI} = 0.018) \tag{11}$$

Table 3. Building Performance Indicator (BPI) records.

System	Jan-17	Jan-19	Jan-21	Apr-22	Jul-22	Oct-22	Feb-23
Structure	80.0	88.0	90.0	90.0	90.0	90.0	90.0
Exterior Envelope	80.7	89.3	82.2	82.2	87.0	87.0	90.0
Interior Finishes	86.2	86.2	86.2	83.7	84.7	84.7	86.7
Power Supply	87.1	84.0	86.2	86.2	86.2	86.2	88.0
Water and Sewerage System	70.0	70.0	70.0	70.0	80.2	85.0	85.0
HVAC	64.8	70.0	90.0	90.0	90.0	90.0	90.0
Fire Detection and Suppression	95.0	95.0	90.0	90.0	90.0	87.0	90.0
Elevators and Escalators	-	-	-	-	-	-	-
Peripheral Infrastructure	90.0	82.5	67.5	67.5	75.0	75.0	75.0
BPI Score	84.0	83.3	85.3	84.5	86.5	86.8	88.1

The rate of the deterioration-over-time coefficient (D) is evaluated based on the infrastructure properties. It is required to determine the factors (SR, EC, and MP) and the corresponding weights (W_{UI}, W_{EC}, W_{MP}). In our case, the service regime is determined as intensive service (4), the environmental conditions are moderate (3), and the material properties are durable materials (2). The weights are equally defined and were set to 1.0. The initial performance (P_0) was set to 1.0, the a_0 set to 10.0, and the designed lifecycle (LC) of the infrastructure was determined to be 75 years. In this case, the P variable was also defined with uncertainty, and the P score was determined as a lognormal distributed variable, as described in Equation (12).

$$P \sim logN\ (\ \mu_P = 3.03, \sigma_P = 0.198) \tag{12}$$

3.3. Risk Calculations

The location of the substation is in the Bik'at HaYarden region. In order to get a full hazard curve for the location, an approximation of the curve was executed based on the Geophysical Institute of Israel (GII) data of the annual-rate ground-motion probabilities of exceedance for 2%, 5%, and 10% probability in 50 years [53]. The full hazard curve is presented in Figure 3.

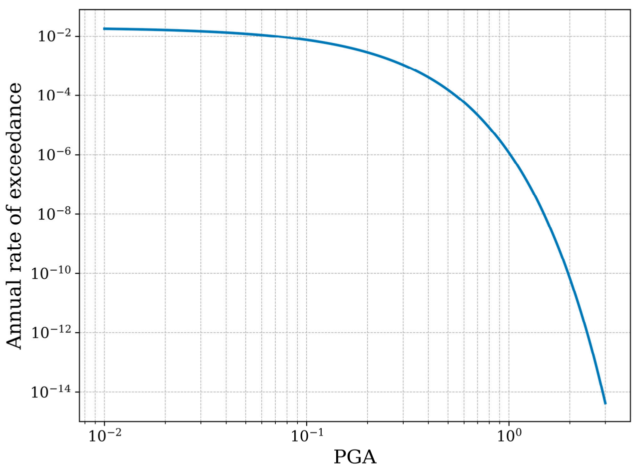

Figure 3. Hazard curve for Bik'at HaYarden region.

In the subsequent phase of our analysis, we computed the risk associated with the substation. To account for uncertainty, a Monte Carlo simulation was utilized. A total of

1000 simulations were performed (n = 1000) for the described case study. Figure 4 presents the variation of the annual risk across 1000 simulations over the lifecycle of the substation. Each simulation is represented in gray, with the mean risk across all simulations highlighted in dark blue. The risk for Year 0 (beginning of Year 1) represents the scenario without considering maintenance and deterioration. Table 4 displays the mean value, standard deviation, minimum and maximum values, as well as the 25th, 50th, and 75th percentile values of the generated data for the BPI and P, and the results for the total risk over the lifecycle (TRLC). For the scope of this case study, we primarily focused on the risk derived from the repair costs of the substation. However, for a comprehensive risk assessment, it is essential to incorporate both direct and indirect impacts, as described in Equation (9).

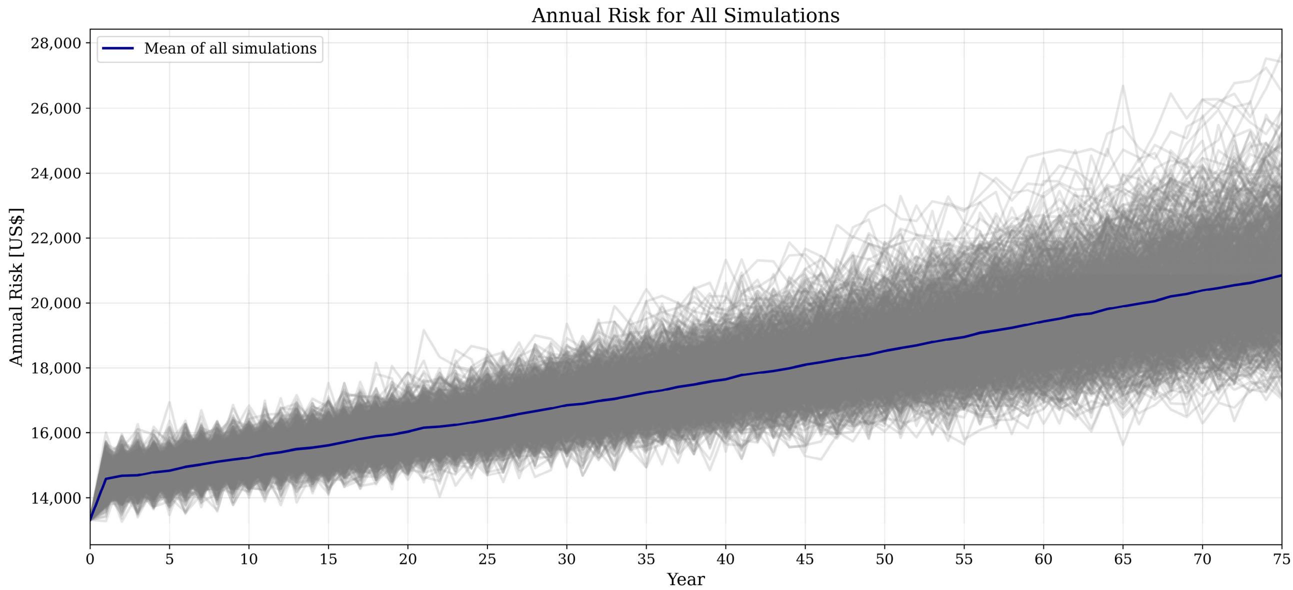

Figure 4. The annual risk over the design lifecycle of the substation. Each simulation is represented in gray. The mean risk highlighted in dark blue. The risk for Year 0 represents the scenario without considering maintenance and deterioration.

Table 4. Simulation values description.

	P	BPI	TRLC (US$)
Mean	21.05	85.45	1,330,458
Std.	4.23	1.57	50,953
Min Value	10.55	80.03	1,205,265
25% (1st Quartile)	17.89	84.39	1,292,154
50% (Median)	20.81	85.35	1,327,313
75% (3rd Quartile)	23.75	86.49	1,362,107
Max Value	38.13	90.27	1,543,828

Furthermore, Figure 5 displays the distribution of the generated P values and BPI values from the Monte Carlo simulation. Meanwhile, Figure 6 illustrates the distribution of the total risk over the lifecycle based on 1000 Monte Carlo simulations. The histogram emphasizes the frequency of various risk outcomes, offering insights into the variance and central tendency of the anticipated lifecycle risks. However, it should be noted that the histograms of the TRLC are not always a good visual for risk managers; therefore, it is proposed to add specific percentiles (90%, 95%, 99%) as a more targeted and actionable metric of risk reliability and power for risk managers. These percentiles can serve as more precise indicators, offering a focused approach to seismic risk evaluation and maintenance planning.

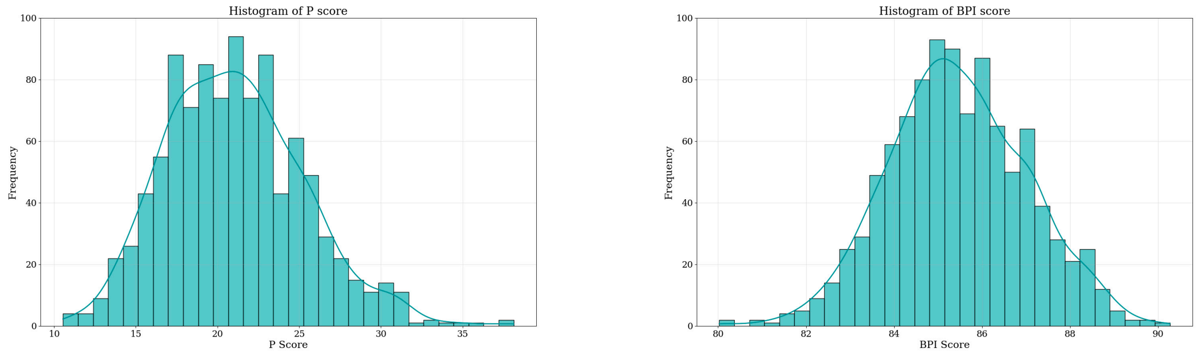

(**a**) (**b**)

Figure 5. Distribution of the generated (**a**) P-score values and (**b**) BPI-score values in the Monte Carlo simulation.

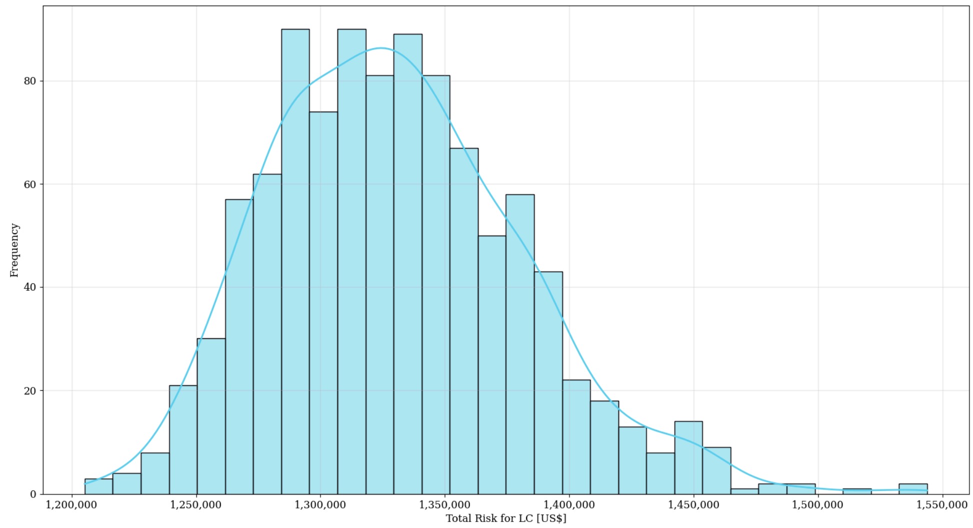

Figure 6. Distribution of the total risk over the lifecycle (TRLC) as obtained from the Monte Carlo simulation.

4. Sensitivity Analysis

In this section, a sensitivity analysis is conducted. Sensitivity analyses assess how varying values of independent variables, such as the BPI score and P score, influence a specific dependent variable. In our context, the dependent variable of interest is the TRLC. Therefore, the sensitivity analysis is aimed at analyzing the BPI score and the P score.

In order to gain a comprehensive understanding of the BPI score's influence, a set of five distinct Monte Carlo simulations were conducted, each with n = 500 trials. These simulations were performed for five different mean BPI-score values: 75, 80, 85, 90, and 95. In this set of simulations, the standard deviation was set at 20% of the mean BPI value, and any generated BPI values exceeding 100 were regenerated. In total, an additional 2500 simulations were carried out.

Figure 7 illustrates the sensitivity of the total risk to variations of the mean BPI. As the mean BPI ascends, there is a discernible decline in the total risk. This inverse relationship suggests that, as the building performance index improves (i.e., increases), the associated risk is reduced. This aligns with the expectation that buildings with superior performance metrics would likely possess a reduced risk of incurring damage or failure. Then, for a deeper understanding of the relationship, and to quantify the change in risk for a unit change in BPI, a regression model was executed. The linear regression model is demonstrated in Figure 7, exhibiting an R^2 value of 0.982. According to the regression model, each unit increase in BPI corresponds to a decrease in risk by USD 13,971. In other words, a change of one unit in the BPI will impact 0.1% of the TRLC. Additionally, Figure 8 presents a box plot illustrating the distribution of the TRLC for each distinct BPI value. The figure presents the median risk, and as the BPI increases, the median risk decreases, aligning with our earlier findings. The height of each box represents the interquartile range (IQR), which is the interval between the 25th and 75th percentiles. The IQR remains relatively consistent across different BPI values, indicating that the spread or variability in risk is consistent. The points outside the whiskers represent potential outliers. It is noticeable that there are some outliers in the data. This indicated the higher possibility of extreme scenarios.

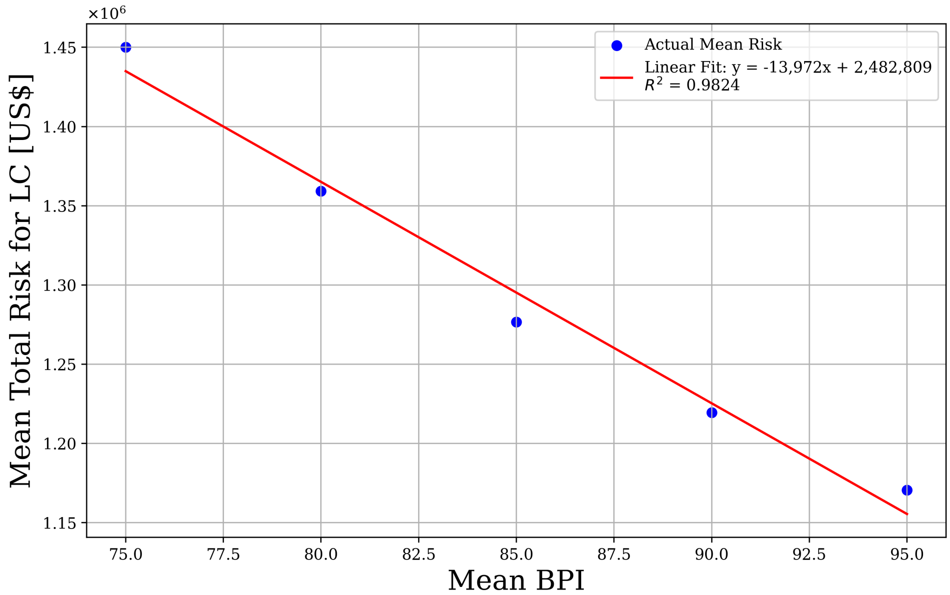

Figure 7. A linear regression model for the relationship between the BPI and the mean total risk over the LC.

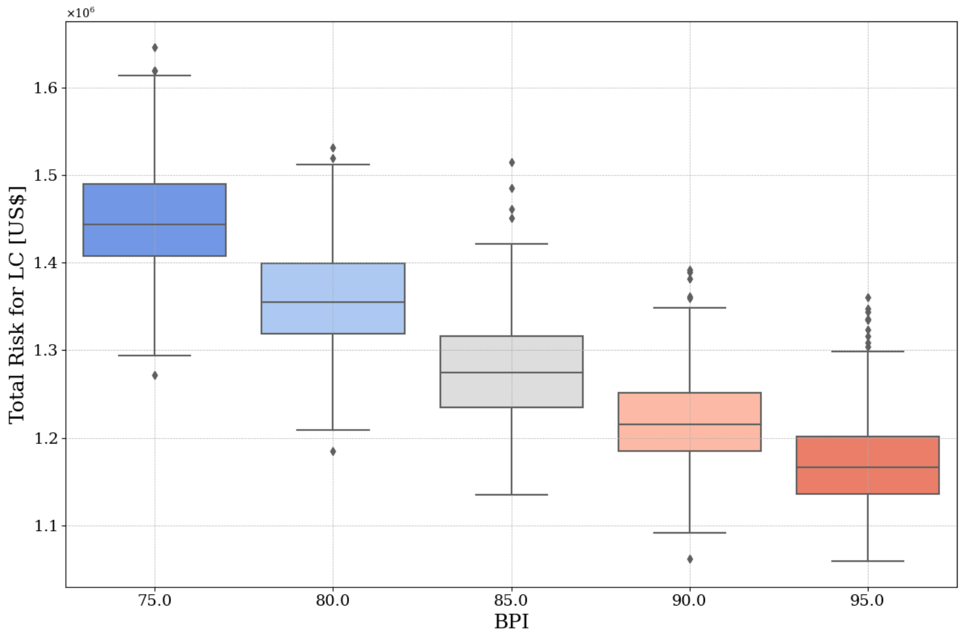

Figure 8. Distribution of the total risk over the lifecycle (LC) across different BPI values. Each box represents the interquartile range (IQR), with the central line indicating the median. Whiskers extend to the range of the data, while outliers are depicted as diamonds outside the whiskers.

Analysis of the distribution of risks for each BPI value was carried out. Table 5 and Figure 9 present the distribution of the TRLC for different BPI values. It can be noticed that, as the BPI increases, there is a shift to the left in the distributions, indicating a decrease in the total risk, which aligns with our earlier findings from the regression analysis. This indicates that effective maintenance significantly mitigates the seismic risk, while lack of maintenance increases the seismic risk.

Table 5. Descriptive statistics of the total risk over the lifecycle (TRLC) for various BPI values, showcasing the mean, standard deviation, minimum, interquartile ranges, and maximum values for each set of simulations (n = 500).

Mean BPI	BPI = 75	BPI = 80	BPI = 85	BPI = 90	BPI = 95
n=	500	500	400,500	500	500
Mean	1,450,061	1,359,205	1,276,655	1,219,459	1,170,639
Std.	62,848	57,358	59,670	51,481	51,742
min.	1,271,963	1,184,940	1,135,168	1,061,887	1,059,202
25%	1,407,262	1,318,910	1,234,882	1,184,530	1,135,560
50%	1,443,205	1,355,042	1,274,359	1,214,930	1,166,577
75%	1,490,181	1,398,849	1,316,040	1,251,680	1,201,536
max.	1,645,999	1,531,222	1,514,449	1,391,572	1,360,661

To analyze the P-score value, an additional five distinct Monte Carlo simulations were carried out, each consisting of n = 400 trials (a total of an additional 2000 simulations). These simulations were implemented for five different mean P-score values. These values were determined based on variations in a single factor, MP. The MP values were set to 1, 2, 3, 4, and 5, corresponding to P scores of 17.42, 21.13, 24.83, 28.54, and 32.25, respectively. Table 6 portrays a summary of the total risk over the lifecycle (TRLC) statistics for the various P scores, detailing the mean, standard deviation, minimum, interquartile ranges, 99th percentile, and maximum values for each simulation set. Figure 10 presents that the linear relationship between the parameter P and the mean total risk over the lifecycle (LC) is evident. An R^2 value of near 1.00 indicates a very strong positive correlation. As the P score increases, there is a corresponding rise in the mean total risk over the LC. In addition, an increase of one unit of the P-score value will increase the TRLC by USD 12,071. Figure 11 provides a detailed perspective of the risk distribution patterns associated with different P values. The figure highlights the variance shift in the TRLC as P increases. For lower P values, the total risk is relatively more concentrated, as shown by the narrower interquartile range (IQR). As P grows, the spread of the risk data becomes more expansive, indicating a broader dispersion and higher variability in the TRLC. This trend is particularly visible in the lengthening of the boxplots' whiskers and the increased number of outliers at higher P values.

Table 6. Descriptive statistics of the total risk over the lifecycle (TRLC) for various P scores, showcasing the mean, standard deviation, minimum, interquartile ranges, 99th percentile, and maximum values for each set of simulations (n = 400).

Mean P	P = 17.42	P = 21.13	P = 24.83	P = 28.54	P = 32.25
n=	400	400	400	400	400
Mean	1,285,687	1,331,761	1,376,718	1,427,703	1,475,491
Std.	40,487	50,175	60,222	72,433	87,367
min.	1,191,755	1,218,358	1,247,397	1,265,752	1,291,696
25%	1,256,330	1,293,241	1,336,244	1,375,846	1,414,411
50%	1,281,857	1,324,765	1,371,375	1,417,702	1,464,657
75%	1,310,973	1,362,096	1,409,387	1,471,124	1,524,204
99%	1,419,327	1,460,045	1,549,155	1,619,376	1,699,655
max.	1,439,320	1,504,185	1,579,054	1,720,524	1,822,565

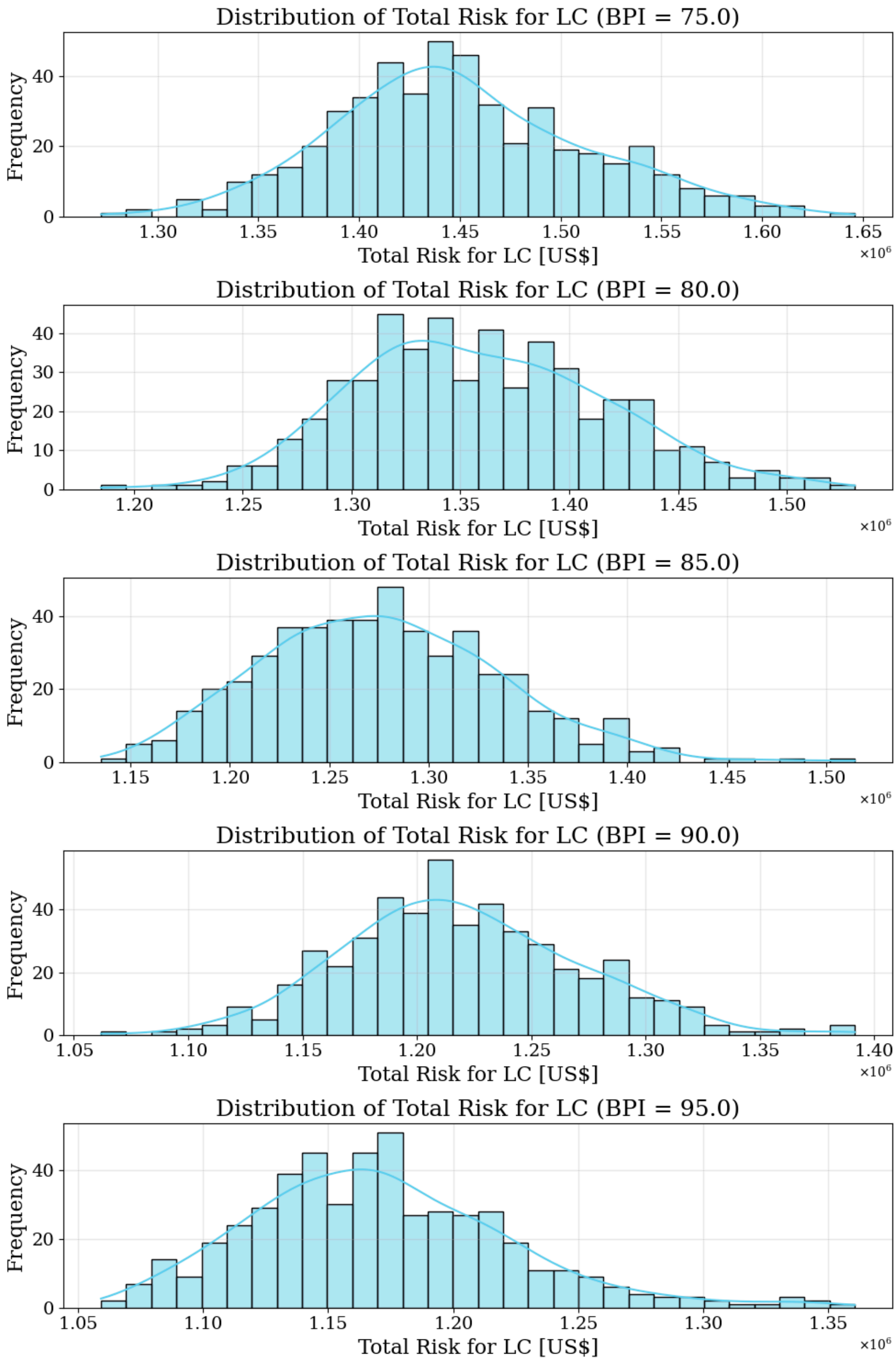

Figure 9. Distributions of the total risk over the lifecycle (TRLC) for different mean BPI values. Each subplot represents the histogram of the TRLC outcomes from the Monte Carlo simulations for a specific mean BPI value.

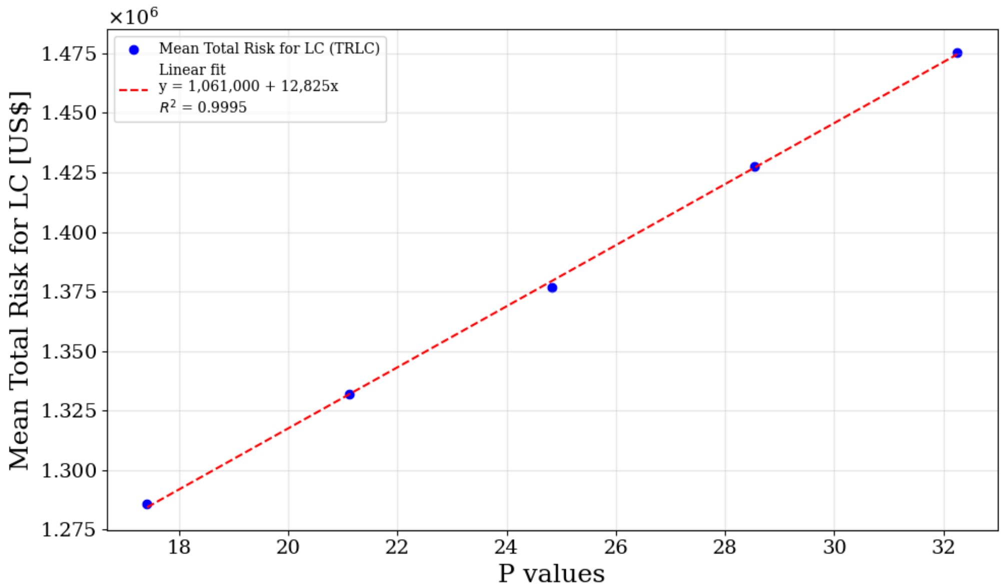

Figure 10. Regression analysis of the relationship between P and the mean total risk over the lifecycle across different simulations. The blue dots represent the mean total risks obtained from simulations at different P values. The red dashed line depicts the linear regression fit, characterized by the equation and a coefficient of determination R^2.

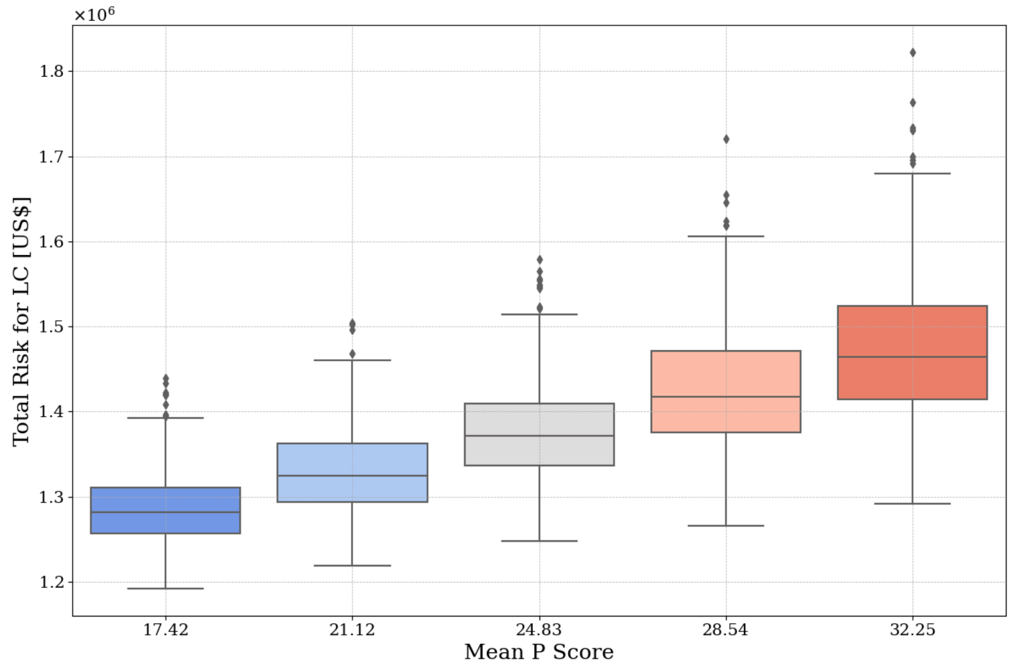

Figure 11. Distribution of the total risk over the lifecycle (LC) across different P values. Each box represents the interquartile range (IQR), with the central line indicating the median. Whiskers extend to the range of the data, while outliers are depicted as diamonds outside the whiskers.

Figure 12 provides a comprehensive visualization of the risk distribution for the lifecycle across a range of P scores. Each histogram represents the frequency distribution of total risks associated with a specific P value. It is noticeable that the distribution of risks shifts as the P value changes; it fits to earlier findings.

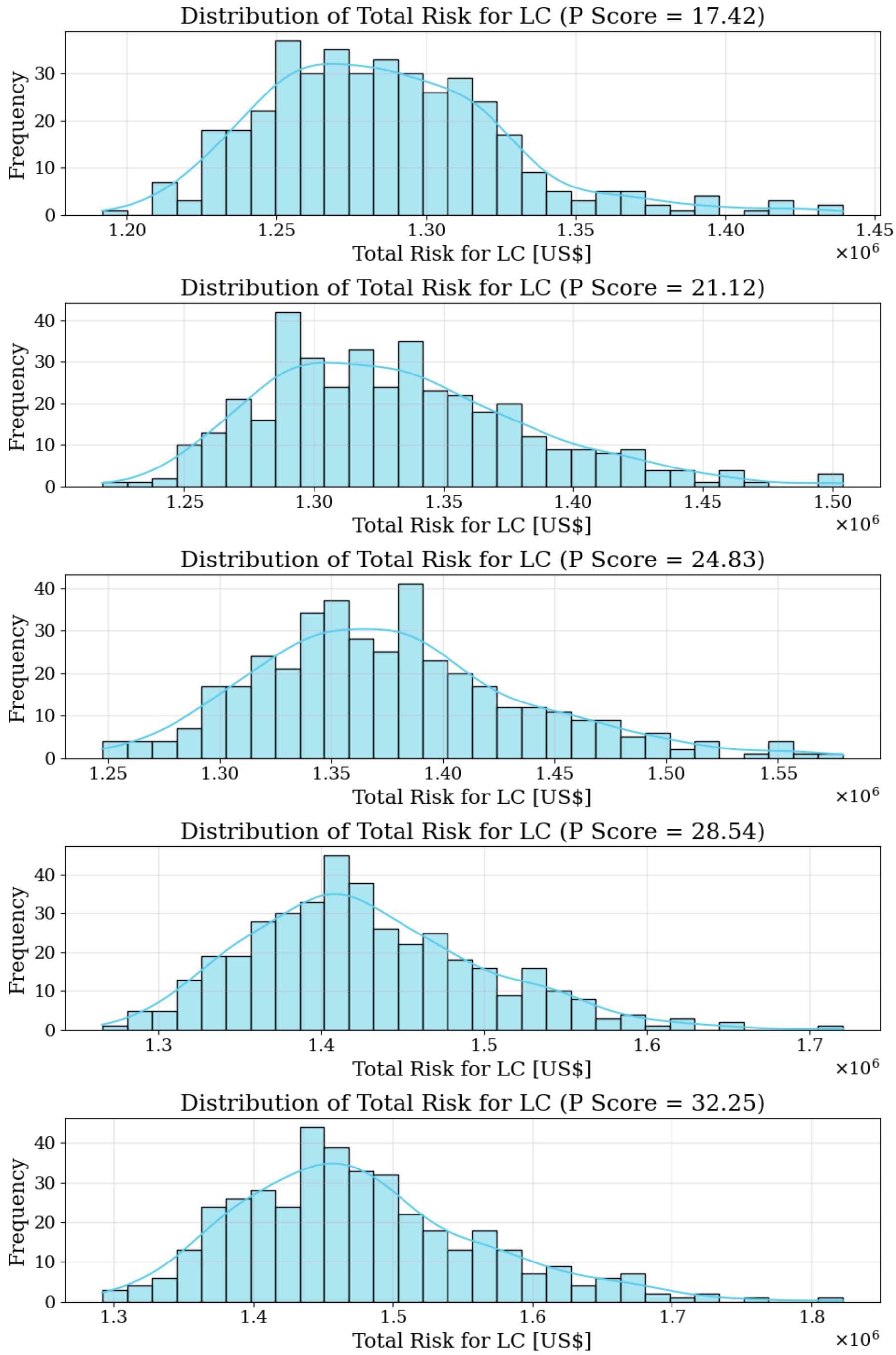

Figure 12. Distributions of the total risk over the lifecycle (TRLC) for different mean P-score values. Each subplot represents the histogram of the TRLC outcomes from the Monte Carlo simulations for a specific mean P-score value.

5. Results and Discussion

The results from the Monte Carlo simulation illustrated a comprehensive analysis of the risk patterns for an infrastructure project spanning a 75-year design lifecycle. These results clarify the interaction between the BPI and P scores and their cumulative effect on the total risk over the lifecycle (TRLC). Specifically, it was observed that both the BPI and the P score possess statistically significant correlations with the TRLC. This finding indicates that, as the infrastructure's performance enhances, there is a concurrent mitigation in the associated risk.

In addition to the primary simulation, a sensitivity analysis was undertaken to delve deeper into the specific influences of the BPI score and the P score on the total risk over the lifecycle (TRLC). This rigorous analysis aimed to recognize the individual and comparative impacts of these two parameters on the overall risk dynamics of the infrastructure project.

The sensitivity analysis relating to the BPI score revealed that, as the BPI score ascends, indicating an enhanced performance index of the infrastructure, there is a concurrent reduction in the associated risk. This trend signifies the inherent balance between infrastructure performance and the potential risks associated with it. A higher BPI score is synonymous with a better-performing infrastructure, and it is intuitively understood that better performance equates to reduced risks. However, the exact quantification and relationship were established through this analysis, enabling more informed decision-making.

The sensitivity analysis concerning the P score highlighted its strong correlation with the TRLC. A notable trend observed was that higher P values, indicative of deteriorating infrastructure conditions, were associated with increased seismic risk variance. Scenarios characterized by elevated P scores intrinsically possess a wider spectrum of potential risks. This suggests that infrastructures in poorer conditions come with greater uncertainties concerning potential risks. In practical terms, for stakeholders or decision-makers, a higher P value does not only translate to an increase in risk, but also signifies a heightened unpredictability in potential outcomes. This insight underscores the importance of robust risk-mitigation strategies, especially in high-P scenarios, to cater to the broader range of potential risks.

6. Practical Applicability of the Research

The methodology proposed in this paper offers a comprehensive approach to assess and manage the seismic risks associated with infrastructure systems, specifically focusing on integrating maintenance considerations with seismic fragility curves. The practical applicability of this research can be broadly classified into the following domains:

- Decision-making for infrastructure maintenance—The framework provides a quantitative basis for making maintenance decisions. By considering not just the structural attributes but also the state of maintenance, decision-makers can allocate resources more efficiently, targeting the most vulnerable components for repair or upgrades.
- Seismic risk assessment—Integrating maintenance factors into seismic fragility curves allows for a more realistic and dynamic evaluation of seismic risks. This approach is precious for areas prone to seismic events, as it enhances preparedness and response strategies.
- Policy and Regulation—Our methodology can serve as a foundation for developing more comprehensive policies and regulations related to infrastructure resilience against seismic events. Regulatory bodies can adopt our study's metrics and indicators for standardization.
- Economic efficiency—The proposed framework enables a more efficient allocation of resources by focusing on both maintenance and seismic resilience, potentially leading to significant cost savings in the long term.

7. Conclusions

This paper aims to contribute to seismic risk management by providing a comprehensive–innovative approach towards earthquake-resilient infrastructure. A novel approach to seismic risk management by integrating maintenance factors into seismic fragility curves is introduced. The model uniquely focuses on both maintenance conditions and natural infrastructure deterioration, offering a holistic perspective on seismic risk assessment.

The methodology is validated through a case study on a low-voltage substation in Bik'at HaYarden, utilizing a Monte Carlo simulation and sensitivity analysis. Findings reveal a significant correlation between maintenance practices and seismic risks, highlighting the importance of maintenance. Poor maintenance was also found to increase uncertainties in seismic risk assessments, emphasizing the need for thorough analysis by stakeholders.

In summation, the essence of this research lies in its revelation of the pivotal role maintenance plays in seismic risk management for infrastructure. By integrating maintenance parameters with seismic considerations, this study paves the way for a more holistic and deeper understanding of infrastructures' earthquake resilience. The implications of this work are profound, presenting stakeholders with a paradigm that emphasizes proactive maintenance as a cornerstone for seismic risk mitigation.

The adaptable framework presented allows for calibration to incorporate new data for robust decision-making. Further work can focus on extending this approach across infrastructure typologies and validation through physical models. This study launches new opportunities for creating earthquake-resilient built environments by bridging the maintenance–seismicity interplay.

8. Limitations

This study is constrained by the lack of comprehensive data to further calibrate the proposed equations. While the methodology was applied to a specific case, the absence of extensive datasets may limit its abstraction. These limitations highlight areas for future research and data-gathering.

Author Contributions: Conceptualization, A.U. and I.M.S.; Methodology, A.U. and I.M.S.; Software, A.U.; Validation, I.M.S.; Formal analysis, I.M.S.; Investigation, A.U.; Data curation, A.U.; Writing—original draft, A.U.; Writing—review and editing, A.U. and I.M.S.; Visualization, A.U.; Supervision, I.M.S. All authors have read and agreed to the published version of the manuscript.

Funding: This research received no external funding.

Data Availability Statement: Not applicable.

Conflicts of Interest: The authors declare no conflict of interest.

Appendix A. Classification and Grading of Service Regime, Environmental Conditions, and Material Properties

Service regime (SR): This is measured on a scale from 1 to 5, where 1 is very-light usage and 5 is very-high usage.

1. Very-light service regime (e.g., a residential road)
2. Light service regime (e.g., a small-town main road)
3. Moderate service regime (e.g., a city street)
4. Intensive service regime (e.g., busy city street)
5. Very-intensive service regime (e.g., a highway or freeway)

Environmental conditions (EC): This is measured on a scale from 1 to 5, where 1 is very-light environmental conditions and 5 is very-harsh conditions.

1. Very-mild conditions (e.g., indoor, climate-controlled, stable temperature and humidity, no exposure to weather or environmental stressors such as extreme wind storms, no heat and tow cycles)
2. Mild conditions (e.g., outdoor in a region with mild weather, moderate temperature and humidity, limited exposure to weather extremes)
3. Moderate conditions (e.g., outdoor with some weather extremes, occasional exposure to high or low temperatures, humidity variations, or mild salinity)
4. Harsh conditions (e.g., outdoor with regular weather extremes, frequent exposure to high or low temperatures, humidity variations, or moderate salinity)
5. Very-harsh conditions (e.g., coastal areas with high salinity, areas with extreme temperatures or humidity, frequent exposure to severe weather conditions)

Material properties (MP). This is measured on a scale from 1 to 5, where 1 is very-durable materials and 5 is materials highly susceptible to deterioration.

1. Extremely durable materials (e.g., advanced composites)
2. Durable materials (e.g., stainless steel, concrete)

3. Moderately durable materials (e.g., steel)
4. Less-durable materials (e.g., URM—unreinforced masonry wall)
5. Highly susceptible to deterioration (e.g., wood, porose concrete)

References

1. Urlainis, A.; Ornai, D.; Levy, R.; Vilnay, O.; Shohet, I.M. Loss and Damage Assessment in Critical Infrastructures Due to Extreme Events. *Saf. Sci.* **2022**, *147*, 105587. [CrossRef]
2. Cinar, E.N.; Abbara, A.; Yilmaz, E. Earthquakes in Turkey and Syria-Collaboration Is Needed to Mitigate Longer Terms Risks to Health. *BMJ* **2023**, *380*, 559. [CrossRef] [PubMed]
3. Gkougkoustamos, I.; Krassakis, P.; Kalogeropoulou, G.; Parcharidis, I. Correlation of Ground Deformation Induced by the 6 February 2023 M7.8 and M7.5 Earthquakes in Turkey Inferred by Sentinel-2 and Critical Exposure in Gaziantep and Kahramanmaraş Cities. *GeoHazards* **2023**, *4*, 267–285. [CrossRef]
4. Cimellaro, G.P.; Reinhorn, A.M.; Bruneau, M. Framework for Analytical Quantification of Disaster Resilience. *Eng. Struct.* **2010**, *32*, 3639–3649. [CrossRef]
5. Rasulo, A.; Pelle, A.; Briseghella, B.; Nuti, C. A Resilience-Based Model for the Seismic Assessment of the Functionality of Road Networks Affected by Bridge Damage and Restoration. *Infrastructures* **2021**, *6*, 112. [CrossRef]
6. Bocchini, P.; Frangopol, D.M.; Ummenhofer, T.; Zinke, T. Resilience and Sustainability of Civil Infrastructure: Toward a Unified Approach. *J. Infrastruct. Syst.* **2014**, *20*, 04014004. [CrossRef]
7. Porter, K. *A Beginner's Guide to Fragility, Vulnerability, and Risk*; Springer: Berlin/Heidelberg, Germany, 2020.
8. National Institute of Building Sciences. HAZUS-MH: Users's Manual and Technical Manuals. In *Report Prepared for the Federal Emergency Management Agency*; Federal Emergency Management Agency: Washington, DC, USA, 2004.
9. Urlainis, A.; Shohet, I.M. Development of Exclusive Seismic Fragility Curves for Critical Infrastructure: An Oil Pumping Station Case Study. *Buildings* **2022**, *12*, 842. [CrossRef]
10. Porter, K.; Kennedy, R.; Bachman, R. Creating Fragility Functions for Performance-Based Earthquake Engineering. *Earthq. Spectra* **2007**, *23*, 471–489. [CrossRef]
11. Porter, K.; Hamburger, R.; Kennedy, R. Practical Development and Application of Fragility Functions. In Proceedings of the Research Frontiers at Structures Congress 2007, Long Beach, CA, USA, 20 June 2007; American Society of Civil Engineers: Long Beach, CA, USA, 2007.
12. Baker, J.W. Efficient Analytical Fragility Function Fitting Using Dynamic Structural Analysis. *Earthq. Spectra* **2015**, *31*, 579–599. [CrossRef]
13. Sandoli, A.; Calderoni, B.; Lignola, G.P.; Prota, A. Seismic Vulnerability Assessment of Minor Italian Urban Centres: Development of Urban Fragility Curves. *Bull. Earthq. Eng.* **2022**, *20*, 5017–5046. [CrossRef]
14. Rosti, A.; Rota, M.; Penna, A. Empirical Fragility Curves for Italian URM Buildings. *Bull. Earthq. Eng.* **2021**, *19*, 3057–3076. [CrossRef]
15. Rosti, A.; Del Gaudio, C.; Rota, M.; Ricci, P.; Di Ludovico, M.; Penna, A.; Verderame, G.M. Empirical Fragility Curves for Italian Residential RC Buildings. *Bull. Earthq. Eng.* **2021**, *19*, 3165–3183. [CrossRef]
16. Ruggieri, S.; Tosto, C.; Rosati, G.; Uva, G.; Ferro, G.A. Seismic Vulnerability Analysis of Masonry Churches in Piemonte after 2003 Valle Scrivia Earthquake: Post-Event Screening and Situation 17 Years Later. *Int. J. Archit. Herit.* **2020**, *16*, 717–745. [CrossRef]
17. Rojas-Mercedes, N.; Erazo, K.; Di Sarno, L. Seismic Fragility Curves for a Concrete Bridge Using Structural Health Monitoring and Digital Twins. *Earthq. Struct.* **2022**, *22*, 503–515. [CrossRef]
18. O'Rourke, M.J.; So, P. Seismic Fragility Curves for On-Grade Steel Tanks. *Earthq. Spectra* **2000**, *16*, 801–815. [CrossRef]
19. Razzaghi, M.S.; Eshghi, S. Development of Analytical Fragility Curves for Cylindrical Steel Oil Tanks. In Proceedings of the 14th World Conference on Earthquake Engineering, Beijing, China, 12–17 October 2008; p. 8.
20. Buratti, N.; Tavano, M. Dynamic Buckling and Seismic Fragility of Anchored Steel Tanks by the Added Mass Method. *Earthq. Eng. Struct. Dyn.* **2014**, *43*, 1–21. [CrossRef]
21. Tseng, C.Y.; Wang, C.H.; Zheng, X.Y.; Chiu, H.C.; Jiang, J.A. Design of a Seismic Hazard Risk Assessment Model for EHV Transmission Grid. In Proceedings of the Second EAI International Conference, SmartGIFT 2017, London, UK, 27–28 March 2017. [CrossRef]
22. Nariman, A.; Fattahi, M.H.; Talebbeydokhti, N.; Sadeghian, M.S. Assessment of Seismic Resilience in Urban Water Distribution Network Considering Hydraulic Indices. *Iran. J. Sci. Technol. Trans. Civ. Eng.* **2022**, *47*, 1165–1179. [CrossRef]
23. Argyroudis, S.; Mitoulis, S.; Kaynia, A.M.; Winter, M.G. Fragility Assessment of Transportation Infrastructure Systems Subjected to Earthquakes. In Proceedings of the GEESD V, Geotechnical Special Publication (GSP 292), Austin, TX, USA, 10–13 June 2018. [CrossRef]
24. Sevieri, G.; De Falco, A.; Marmo, G. Shedding Light on the Effect of Uncertainties in the Seismic Fragility Analysis of Existing Concrete Dams. *Infrastructures* **2020**, *5*, 22. [CrossRef]
25. Frangopol, D.M.; Saydam, D.; Kim, S. Maintenance, Management, Lifecycle Design and Performance of Structures and Infrastructures: A Brief Review. *Struct. Infrastruct. Eng.* **2012**, *8*, 1–25. [CrossRef]
26. Soleimanmeigouni, I.; Ahmadi, A.; Kumar, U. Track Geometry Degradation and Maintenance Modelling: A Review. *Proc. Inst. Mech. Eng. Part F* **2018**, *232*, 73–102. [CrossRef]

27. Sedghi, M.; Kauppila, O.; Bergquist, B.; Vanhatalo, E.; Kulahci, M. A Taxonomy of Railway Track Maintenance Planning and Scheduling: A Review and Research Trends. *Reliab. Eng. Syst. Saf.* **2021**, *215*, 107827. [CrossRef]
28. Volovski, M.; Murillo-Hoyos, J.; Saeed, T.U.; Labi, S. Estimation of Routine Maintenance Expenditures for Highway Pavement Segments: Accounting for Heterogeneity Using Random-Effects Models. *J. Transp. Eng. Part A* **2017**, *143*, 04017006. [CrossRef]
29. Woldemariam, W.; Murillo-Hoyos, J.; Labi, S. Estimating Annual Maintenance Expenditures for Infrastructure: Artificial Neural Network Approach. *J. Infrastruct. Syst.* **2016**, *22*, 04015025. [CrossRef]
30. Verdezoto, N.; Bagalkot, N.; Akbar, S.Z.; Sharma, S.; MacKintosh, N.; Harrington, D.; Griffiths, P. The Invisible Work of Maintenance in Community Health: Challenges and Opportunities for Digital Health to Support Frontline Health Workers in Karnataka, South India. *Proc. ACM Hum.-Comput. Interact.* **2021**, *5*, 1–31. [CrossRef]
31. Caldera, S.; Mostafa, S.; Desha, C.; Mohamed, S. Integrating Disaster Management Planning into Road Infrastructure Asset Management. *Infrastruct. Asset Manag.* **2021**, *8*, 219–233. [CrossRef]
32. Lei, X.; Sun, L.; Xia, Y. Seismic Fragility Assessment and Maintenance Management on Regional Bridges Using Bayesian Multi-Parameter Estimation. *Bull. Earthq. Eng.* **2021**, *19*, 6693–6717. [CrossRef]
33. Zanini, M.A.; Faleschini, F.; Pellegrino, C. Cost Analysis for Maintenance and Seismic Retrofit of Existing Bridges. *Struct. Infrastruct. Eng.* **2016**, *12*, 1411–1427. [CrossRef]
34. Shohet, I.M. Building Evaluation Methodology for Setting Maintenance Priorities in Hospital Buildings. *Constr. Manag. Econ.* **2003**, *21*, 681–692. [CrossRef]
35. Manos, G.C.; Simos, N.; Kozikopoulos, E. The Structural Performance of Stone-Masonry Bridges. In *Structural Bridge Engineering*; IntechOpen: London, UK, 2016. [CrossRef]
36. Crespi, P.; Zucca, M.; Valente, M.; Longarini, N. Influence of Corrosion Effects on the Seismic Capacity of Existing RC Bridges. *Eng. Fail. Anal.* **2022**, *140*, 106546. [CrossRef]
37. Zanini, M.A.; Pellegrino, C.; Morbin, R.; Modena, C. Seismic Vulnerability of Bridges in Transport Networks Subjected to Environmental Deterioration. *Bull. Earthq. Eng.* **2013**, *11*, 561–579. [CrossRef]
38. Soltani, M.; Raissi Dehkordi, M.; Eghbali, M.; Samadian, D.; Salmanmohajer, H. Influence of Infill Walls on Resilience Index of RC Schools Using the BIM Analysis and FEMA P-58 Methodology. *Int. J. Civ. Eng.* **2022**, *21*, 711–726. [CrossRef]
39. Tecchio, G.; Donà, M.; Saler, E.; da Porto, F. Fragility of Single-Span Masonry Arch Bridges Accounting for Deterioration and Damage Effects. *Eur. J. Environ. Civ. Eng.* **2022**, *27*, 2048–2069. [CrossRef]
40. Wang, K.C.; Almassy, R.; Wei, H.H.; Shohet, I.M. Integrated Building Maintenance and Safety Framework: Educational and Public Facilities Case Study. *Buildings* **2022**, *12*, 770. [CrossRef]
41. Urlainis, A.; Shohet, I.M. Probabilistic Risk Appraisal and Mitigation of Critical Infrastructures for Seismic Extreme Events. In Proceedings of the Creative Construction Conference (CCC2018), Ljubljana, Slovenia, 30 June–3 July 2018. [CrossRef]
42. Urlainis, A.; Shohet, I.M. Seismic Risk Mitigation and Management for Critical Infrastructures Using an RMIR Indicator. *Buildings* **2022**, *12*, 1748. [CrossRef]
43. Wei, H.H.; Skibniewski, M.J.; Shohet, I.M.; Shapira, S.; Aharonson-Daniel, L.; Levi, T.; Salamon, A.; Levy, R.; Levi, O. Benefit-Cost Analysis of the Seismic Risk Mitigation for a Region with Moderate Seismicity: The Case of Tiberias, Israel. *Procedia Eng.* **2014**, *85*, 536–542. [CrossRef]
44. Nuti, C.; Rasulo, A.; Vanzi, I. Seismic Safety Evaluation of Electric Power Supply at Urban Level. *Earthq. Eng. Struct. Dyn.* **2007**, *36*, 536–542. [CrossRef]
45. Nuti, C.; Rasulo, A.; Vanzi, I. Seismic Safety of Network Structures and Infrastructures. *Struct. Infrastruct. Eng.* **2010**, *6*, 95–110. [CrossRef]
46. Rasulo, A.; Nardoianni, S.; Evangelisti, A.; D'Apuzzo, M. Incorporating Traffic Models into Seismic Damage Analysis of Bridge Road Networks: A Case Study in Central Italy. *Infrastructures* **2023**, *8*, 113. [CrossRef]
47. Federal Emergency Management Agency. *Seismic Performance Assessment of Buildings—FEMA P-58*; Federal Emergency Management Agency: Washington, DC, USA, 2012.
48. Mitelman, A.; Lifshitz Sherzer, G. Coupling Numerical Modeling and Machine-Learning for Back Analysis of Cantilever Retaining Wall Failure. *Comput. Concr.* **2023**, *31*, 307–314. [CrossRef]
49. Mitelman, A.; Yang, B.; Urlainis, A.; Elmo, D. Coupling Geotechnical Numerical Analysis with Machine Learning for Observational Method Projects. *Geosciences* **2023**, *13*, 196. [CrossRef]
50. Mitelman, A.; Urlainis, A. Investigation of Transfer Learning for Tunnel Support Design. *Mathematics* **2023**, *11*, 1623. [CrossRef]
51. Dabiri, H.; Faramarzi, A.; Dall'Asta, A.; Tondi, E.; Micozzi, F. A Machine Learning-Based Analysis for Predicting Fragility Curve Parameters of Buildings. *J. Build. Eng.* **2022**, *62*, 105367. [CrossRef]
52. National Institute of Building Sciences. *Hazus Earthquake Model Technical Manual Hazus 4.2 SP3*; National Institute of Building Sciences: Washington, DC, USA, 2020.
53. Klar, A.; Meirova, T.; Zaslavsky, Y.; Shapira, A. *Spectral Acceleration Maps for Use in SI 413 Amendment No.5*; The Geophysical Institute of Israel: Jerusalem, Israel, 2011.